Computational Study of the Adsorption of Trichlorophosphate, Dimethyl Methylphosphonate, and Sarin on Amorphous SiO$_2$

V. M. Bermudez*

Electronics Science and Technology Division, Naval Research Laboratory, Washington, DC 20375-5347

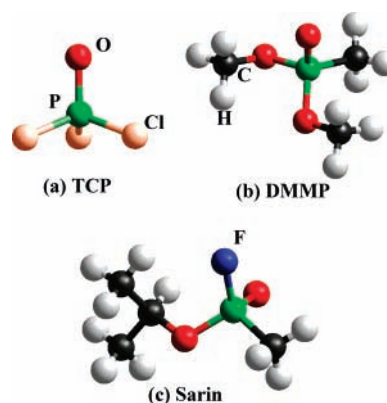*Received: February 23, 2007; In Final Form: April 19, 2007*

Ab initio quantum chemical calculations have been performed to study the adsorption of trichlorophosphate, dimethyl methylphosphonate, and Sarin via hydrogen bonding to Si−OH groups on the amorphous SiO$_2$ (*a*-SiO$_2$) surface. Two SiO$_2$ models are used: a small Si$_5$O$_7$H$_8$ "cagelike" cluster and a larger Si$_{21}$O$_{56}$H$_{28}$ structure designed to approximate the local environment in *a*-SiO$_2$. In the latter case, regions of different local OH density are considered as adsorption sites. Adsorption energies, bonding geometries, and adsorbate vibrational modes are obtained, and anharmonicity is explicitly included in the treatment of the SiO−H stretching mode. The computed results for the adsorption-induced shift in frequency of the SiO−H stretch and of the molecular P=O stretch are compared with the available experimental data. For all three species, the most stable adsorption geometry involves hydrogen bonding between two Si−OH groups and the O atom of the P=O group.

1. Introduction

The interaction of chemical warfare agents (CWAs) with materials is an important issue in protection and remediation. Of specific concern is a basic understanding of the long-term stability of such species (termed "agent fate") under environmental conditions and of the nature of the chemisorption bond at the material surface. These subjects are difficult to address experimentally because of the extreme hazards in working with real CWAs. Relatively benign simulants are typically used instead, but it is often uncertain the extent to which such species mimic the adsorption properties of real CWAs. A direct evaluation of a particular simulant involves, again, experimentation with the corresponding real agent.

An obvious approach to this problem is to apply quantum chemical (QC) methods to model the systems of interest. This has been done in a number of cases[1−11] involving mainly the interaction of CWAs with ionic oxides or with molecular species. For most metal oxides, adsorption generally involves Lewis acid−base chemistry for OH-free surfaces and Brønsted acid−base chemistry for hydroxylated surfaces. On the other hand, for SiO$_2$ and related materials hydrogen bonding (H bonding) to surface silanol (Si−OH) groups is involved, and accurate theoretical treatment of these relatively weak surface H bonds can be difficult.[12] Recently the adsorption, via H bonding, of CWAs on aluminosilicate clay surfaces has been modeled.[3,9] The structures formed are complex and depend on the extent of hydroxylation of the surface.

The present work applies ab initio QC methods to the interaction of three related phosphate and phosphonate molecules on amorphous silica (*a*-SiO$_2$). These are (Figure 1) trichlorophosphate [Cl$_3$P=O, TCP], dimethyl methylphosphonate [(CH$_3$O)$_2$-(CH$_3$)P=O, DMMP] and Sarin [(iPrO)(CH$_3$)(F)P=O, where iPr ≡ (CH$_3$)$_2$CH-]. TCP is used here as a relatively simple species

* To whom correspondence should be addressed. E-mail: victor. bermudez@nrl.navy.mil. Phone: +1-202-767-6728. Fax: +1-202-767-1165.

Figure 1. Schematic diagram of the molecular structures of TCP, DMMP, and Sarin.

for testing the computational procedures and for probing the reactivity of various parts of the model clusters. DMMP is important as a safe simulant for the nerve agent Sarin. The main focus of this work is in comparing theoretical results for the adsorption of TCP and DMMP on *a*-SiO$_2$ with experimental data, especially the infrared (IR) vibrational spectrum and in comparing results for the adsorption of DMMP versus Sarin. The goals are an evaluation of the reliability of QC methods in describing the adsorption and also a "side-by-side" comparison of the behavior of the simulant and the real agent.

2. Computational Methods

All calculations were done using the *Gaussian03* suite of programs[13] with standard basis sets built into the package. Most of the work was done with 6-31$^+$G(2d,2p) basis sets, but some results were obtained for comparison at the 6-311^{++}G(d, p) and 6-31$^+$G(d, p) levels. It is clear from previous work[14,15] that heavy-atom diffuse functions, together with polarization functions both on heavy atoms and on H, are necessary for an

Report Documentation Page

1. REPORT DATE **APR 2007**	2. REPORT TYPE	3. DATES COVERED **00-00-2007 to 00-00-2007**

4. TITLE AND SUBTITLE	5a. CONTRACT NUMBER
Computational Study of the Adsorption of Trichlorophosphate, Dimethyl Methylphosphonate, and Sarin on Amorphous SiO2	5b. GRANT NUMBER
	5c. PROGRAM ELEMENT NUMBER
6. AUTHOR(S)	5d. PROJECT NUMBER
	5e. TASK NUMBER
	5f. WORK UNIT NUMBER

7. PERFORMING ORGANIZATION NAME(S) AND ADDRESS(ES) **Naval Research Laboratory,Electronics Science and Technology DiVision,4555 Overlook Avenue SW,Washington,DC,20375**	8. PERFORMING ORGANIZATION REPORT NUMBER

9. SPONSORING/MONITORING AGENCY NAME(S) AND ADDRESS(ES)	10. SPONSOR/MONITOR'S ACRONYM(S)
	11. SPONSOR/MONITOR'S REPORT NUMBER(S)

12. DISTRIBUTION/AVAILABILITY STATEMENT **Approved for public release; distribution unlimited**

13. SUPPLEMENTARY NOTES

14. ABSTRACT

15. SUBJECT TERMS

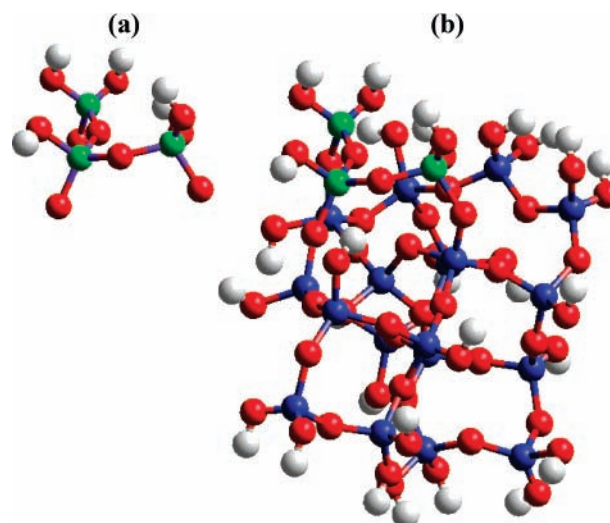| 16. SECURITY CLASSIFICATION OF:			17. LIMITATION OF ABSTRACT	18. NUMBER OF PAGES	19a. NAME OF RESPONSIBLE PERSON
a. REPORT **unclassified**	b. ABSTRACT **unclassified**	c. THIS PAGE **unclassified**	**Same as Report (SAR)**	**10**	

adequate description of H bonding in the present case. Hence, 6-31⁺G(d, p) is considered to be the smallest basis set that can be used reliably. It has also been shown[15] in studies of NH_3 adsorption on SiO_2 that 6-31⁺G(2d,2p) basis sets yield a somewhat more accurate adsorption energy (ΔE_{ads}, see below) than do 6-31⁺G(d, p) but that further enlargement, up to 6-311⁺⁺G(2d,2p), has no significant additional effect on ΔE_{ads}. All calculations were done using density functional theory (DFT) with the B3LYP functional. In the past, questions have sometimes been raised concerning the applicability of DFT to H bonding. However, several previous studies (e.g., refs 14–20) have demonstrated the validity of DFT with the B3LYP functional in describing the H bonding of adsorbates (including phosphonates[14,19]) on SiO_2 surfaces.

Much of the present work involves a comparison of observed and calculated IR vibrational spectra as a means of evaluating the computational methods and results. Particular attention is given to the shift to lower frequency, $\Delta\nu(O-H)$, of the SiO–H stretch that results from adsorption. Previous work[15,16,21] has shown that accurate results for $\Delta\nu(O-H)$ require that anharmonicity be treated explicitly. Computation of anharmonic terms for all 3N-6 modes of an N-atom model (adsorbate plus SiO_2 cluster) is not feasible for systems of the size studied here; therefore, the approach described previously[22] is followed. The $\nu(O-H)$ mode is well separated in energy from (and therefore decoupled from) all other modes. Beginning with the relaxed structure, a series of single-point calculations is done in which the H atom is displaced incrementally in a direction parallel to the O–H bond. In total, 28 displacements in the range of $-0.55 \leq \delta_{O-H} \leq +0.85$ Å, relative to the equilibrium O–H distance of about 0.96 Å, were used.

The one-dimensional (1D) energy surface thus obtained was least-squares fitted with a polynomial of order $12 \leq k \leq 15$ in δ_{OH}, and the resulting potential function was then used to solve the 1D Schrödinger equation numerically.[23] A high-k polynomial was necessary to optimize the fit over a wide range of δ_{O-H}. A similar procedure was also used to estimate the effects of anharmonicity in the P=O stretching mode of TCP. The mass used for the oscillator is the reduced mass, $\mu_{XY} = (m_X m_Y)/(m_X + m_Y)$. From the lowest three eigenvalues (E_0, E_1, and E_2) the quantities of interest are obtained. These are the anharmonic fundamental and first-overtone frequencies $\nu_{01} = (E_1 - E_0)$ and $\nu_{02} = (E_2 - E_0)$ and the anharmonicity parameter $\nu_e x_e = (2\nu_{01} - \nu_{02})/2$ where ν_e is the harmonic frequency.

The approach described above involves an approximation that should be valid in the case of $\nu(O-H)$. In obtaining the 1D potential energy surface, the bond stretching is modeled entirely in terms of H-atom displacement; whereas, the true normal mode is more accurately described in terms of the individual atomic displacements as $\delta_{O-H} = 0.94\delta_H - 0.06\delta_O$. Different effects on the total energy are expected for equivalent displacements of H and O (δ_H and δ_O), but any error in the 1D potential function resulting from the approximation $\delta_{O-H} \approx \delta_H$ has been neglected.

The frequencies of other modes are obtained in the harmonic approximation and scaled using factors given in previous work. The scaling accounts for anharmonicity in an approximate manner, based on an average correction for a wide range of molecules and normal modes. For B3LYP/6-31⁺G(d, p) the factor[24] is 0.9632, and for B3LYP/6-311⁺⁺G(d, p) the factor[25] is 0.9679. To our knowledge, no scaling factor has been reported specifically for B3LYP/6-31⁺G(2d,2p); hence the factor of 0.9632 for B3LYP/6-31⁺G(d, p) will be used. The uncertainty in these factors is in the range of ±0.02–0.03 (ref 24).

Figure 2. Schematic diagram of the model *a*-SiO₂ cluster. A model reactive region with a relatively high OH density is shown in (a). The same reactive region is shown in (b) as part of the total cluster. Si (O) atoms are shown in blue (red) except for the Si atoms at the reactive region which are in green. H atoms are gray. The structure shown in (a) constitutes the ONIOM model system, and the structure shown in (b) is the ONIOM real system. Further details are given in the text.

Other results of interest are ΔE_{ads} and related quantities, defined by

$$\Delta E_{ads} = E(mol + cluster) - E(mol) - E(cluster)$$

$$\Delta E_{ads}^C = \Delta E_{ads} + \Delta E_{BSSE}$$
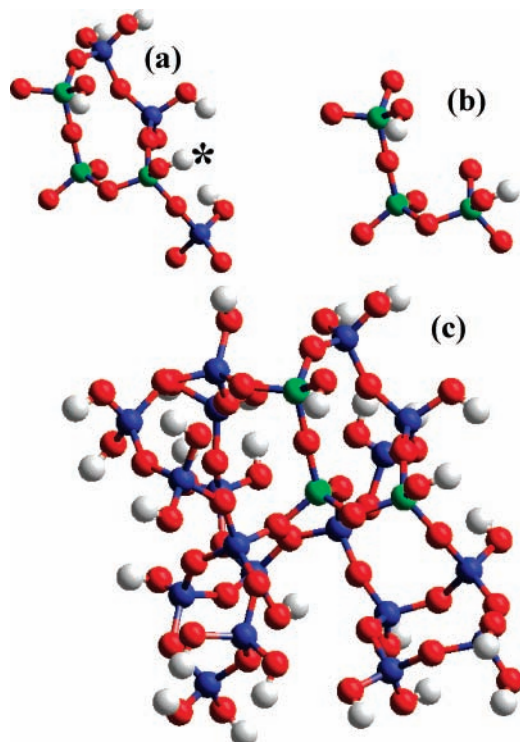
$$\Delta H_{ads}^0 = \Delta E_{ads}^C + \Delta E_{ZPE}$$

where the first term in ΔE_{ads} is the total energy of the relaxed adsorption system and the next two are the relaxed energies of the isolated molecule and cluster. ΔE_{BSSE} is the correction for basis set superposition error (BSSE), which is obtained via the usual counterpoise method. In general, no correction is applied for zero-point vibrational energy (ZPE); however, an estimate of the magnitude of ΔE_{ZPE} will be given below. A negative ΔH_{ads}^0 constitutes an exothermic process.

3. Construction of the Model

3.1. The *a*-SiO₂ Model. The *a*-SiO₂ lattice has been modeled by Van Ginhoven et al.[26] who showed that the physical properties of the bulk glass can be accurately described by averaging over a finite set of three-dimensionally periodic structures formed from properly constructed small cells. Each cell is formed by cooling (in a molecular dynamics (MD) calculation) a gas of 24 Si and 48 O atoms under control of an empirical potential energy function. Constraints are imposed only on the atom density and on the minimum Si–O, O–O, and Si–Si nearest-neighbor distances. Because the process is random, each 72 atom $Si_{24}O_{48}$ cell is unique and represents an arbitrarily chosen small piece of the bulk glass. In modeling bulk glass,[26] each of ten different cells synthesized in this manner is then used to form a "crystal" with periodic boundary conditions and subjected to further annealing using a DFT MD treatment. The average structural properties (radial distribution function, ring size distribution, etc.) of these ten different glasses are in excellent agreement with experiment and with empirical MD simulations for much larger samples (493 SiO_2 units).

The present work uses one of the 72 atom clusters as the model system (cf. Figures 2 and 3) from which are cut small

Figure 3. Similar to Figure 2 but showing a reactive region with a relatively low OH density. Diagrams (a) and (b) show large and small models for the reactive region, respectively. The asterisk in (a) marks the OH site used for TCP adsorption (see text). Si atoms that are common to all three diagrams are shown in green. In (c), the view is from a perspective different from that in Figure 2b.

sections to represent the reactive adsorption sites. A similar approach has already been used[27] to treat the self-trapped exciton in SiO_2. The model is essentially a cluster of finite size that, to the extent possible, exhibits structural characteristics expected for an a-SiO_2 surface. This includes a distribution of different Si−OH configurations as well as siloxane rings of varying size and shape. Hence, the model permits a comparison of the adsorption characteristics of several different types of surface sites with no alteration of the model itself. The present approach differs from that of other studies in which a-SiO_2 is modeled as a small cluster containing only a few SiO_4 tetrahedra (sometimes only one) or as a crystalline structure with a single, well-defined siloxane ring geometry. A similar structure,[28] an OH-free $Si_{24}O_{48}$ cluster, has been used to treat the reaction of H_2O with defects on the a-SiO_2 surface. Here, the model was formed by cutting an $Si_{24}O_{48}$ cluster from crystalline α-quartz and then subjecting it to simulated annealing.

In the present case, all dangling Si (O) bonds on the periphery of the cluster were saturated with OH (H). Dangling −O−Si(OH)$_3$ units, which are known[29] to be unstable on the a-SiO_2 surface above ∼300 °C, were removed and replaced with −OH. The resulting cluster then has a stoichiometry of $Si_{21}O_{56}H_{28}$. Next, the positions of the O and H atoms in the OH groups were optimized at either the semiempirical PM3 level[30] or the ab initio restricted Hartree−Fock (RHF)/3-21G level while the rest of the cluster remained fixed. Two reactive sites were then selected. One (Figure 2a) is a site of relatively high OH density and consists of an isolated (−O−)$_3$Si−OH with adjacent geminal (−O−)$_2$Si(OH)$_2$ groups. The other (Figure 3a,b) is a site of relatively low OH density and consists mainly of isolated Si−OH groups. Many other combinations of isolated and geminal groups are possible, but these two have been chosen as representative of the hydroxylated a-SiO_2 surface

(see below). A fully dehydroxylated a-SiO_2 surface, with only (−O−)$_3$Si−O−Si(−O−)$_3$ bridges, does not occur naturally and requires vacuum annealing[31,32] at ∼1000 °C to form.

The OH density on a fully hydroxylated a-SiO_2 surface has been found experimentally[32] to be ∼5 OH nm^{-2}. Heating in vacuo to ∼450 °C is a typical substrate pretreatment in IR studies of TCP and DMMP adsorption (see below). This desorbs any physisorbed H_2O and converts most H-bonded Si−OH groups to Si−O−Si bridges via H_2O elimination, leaving a coverage of non-H-bonded groups[32] equal to about 2 OH nm^{-2}. For the model used here, the total coverage is about 4.0 OH nm^{-2}, based on the surface area of a sphere enclosing the cluster. The cluster consists predominantly of isolated and geminal Si−OH groups, and only two pairs of Si−OH groups are sufficiently close to H bond to each other. The O−H bond length between two H-bonded silanol sites is taken here to be 2.0 Å, based on results[18] at the MP2/6-31G(d) level for H_2O and CH_3OH interacting with Si(OH)$_4$. Such sites are not used in the present work because the available experimental data for TCP and DMMP adsorption (see below) all focus on a-SiO_2 surfaces with a low coverage of H-bonded OH groups. If the H-bonded sites are excluded, the coverage on the model cluster becomes about 3.4 OH nm^{-2}. Hence, the model corresponds fairly closely to the surfaces used in experimental studies, although the coverage of non-H-bonded Si−OH groups is ∼50% higher than on the real material.

3.2. ONIOM Treatment. In the next step, an ONIOM procedure[33] is applied in which the small reactive-site subcluster (Figure 2a or 3a,b) and the adsorbate define the "model system" while the entire cluster plus adsorbate comprises the "real system". During geometry optimization, all atoms in the ONIOM model system are allowed to relax without constraint while the rest of the cluster remains fixed in position to prevent distortion of the cluster from its bulk-glass configuration. The ONIOM energy is then given by $E = E_{real}^{low} + E_{model}^{high} - E_{model}^{low}$. "Low" refers to a low-level treatment which, in the present work, is either semiempirical (PM3[30] or MNDO[34]) or ab initio (RHF/3-21G). "High" refers to a high-level ab initio treatment which, in the present work, is mainly at the B3LYP/6-31$^+$G(2d,2p) level with an "ultrafine" integration grid and "tight" convergence criteria for geometry optimization to increase the level of accuracy in the treatment of weak H-bonding interactions. Thus, in the definition of ΔE_{ads} given above, $E(mol + cluster)$ is the ONIOM energy with the adsorbate present, and $E(cluster)$ is the ONIOM energy without the adsorbate. The effects of the choice of high- and low-level method will be discussed below. Because of program limitations, ΔE_{BSSE} cannot be obtained directly for an ONIOM model. Hence, after optimizing the ONIOM adsorption structure the model system is detached and H atoms used to saturate the dangling Si−O bonds. The counterpoise procedure is then applied to this isolated structure to get ΔE_{BSSE}. Hydrogen link atoms were used in calculations for the ONIOM model system.

Solans-Monfort et al.[35] have compared ONIOM and periodic− lattice calculations for the adsorption of NH_3 or H_2O at acidic OH sites in the aluminosilicate material "chabazite". They concluded that the two approaches give comparable geometries but that use of RHF/3-21G, rather than a semiempirical method, as the ONIOM low-level method is needed to obtain ΔE_{ads} in agreement with the periodic−lattice result. Furthermore, it was found that good ONIOM results could be obtained by optimizing the geometry using MNDO as the low-level method followed by a single-point calculation with RHF/3-21G as the low-level method. Such single-point calculations of ΔE_{ads} converged

Adsorption of TCP, DMMP, and Sarin on Amorphous SiO₂

J. Phys. Chem. C, Vol. 111, No. 26, 2007 **9317**

rapidly to the periodic−lattice result as the size of the ONIOM model system increased. As a low-level method, MNDO appeared to be somewhat superior to AM1. It should be noted that a periodic−lattice approach might not be practicable for the adsorbates of interest here. Most CWA molecules are even larger than Sarin (Figure 1), and very large unit cells would be required to prevent interaction between nearest-neighbor adsorbates.

Conclusions similar to those mentioned above were reached by Roggero et al.[20] who compared ONIOM results for a "cagelike" cluster model of SiO₂ with those obtained in a fully ab initio, high-level treatment of the entire cluster. In particular, it was found that ONIOM results with RHF/3-21G as the low-level method were in excellent agreement with those for the fully high-level treatment and that the ONIOM results converged rapidly as the size of the model system increased. It was also found[20] that PM3 performs relatively poorly as an ONIOM low-level method for SiO₂. However, Michalkova et al.[3] found that PM3 and RHF/3-21G give similar results when used as the ONIOM low-level method in modeling adsorption of Sarin on the aluminosilicate material "dickite". The difference may be related to the size of the ONIOM model system, which was quite large in ref 3 versus here and in ref 20. It is likely that with a sufficiently large model system the accuracy of the low-level method becomes relatively unimportant. A comparison of AM1, PM3, and MNDO/d in predicting the structures of small Si-containing molecules has also been given by Bartlett et al.[36]

In the present work, a calculation for the bare (i.e., adsorbate-free) cluster (Figure 2a) with PM3 as the ONIOM low-level method and B3LYP/6-31⁺G(2d,2p) for the high-level gave a Mulliken charge of $q_{Si}^{model} = +1.28$ |e| for Si atoms in the model system. The same calculation with MNDO (RHF/3-21G) as the low-level method gave $q_{Si}^{model} = +1.83$ |e| (+2.03 |e|). The RHF/3-21G result is virtually identical to the Mulliken charge of +2.036 |e| found in a periodic RHF treatment[37] of bulk α-SiO₂. Hence, q_{Si}^{model} is sensitive to the choice of low-level method, and even a simple ab initio method gives a charge result close to that obtained for a bulk lattice. Further discussion is given below regarding the different results obtained for the three low-level methods.

4. Results and Discussion

4.1. TCP Adsorbed on *a*-SiO₂. The main interest in the present work is in the adsorption of phosphonates on the hydroxylated *a*-SiO₂ surface. To our knowledge there are few previous theoretical studies[14,19] of this particular problem. The adsorption of TCP was taken as a starting point because it is a smaller and simpler molecule than either DMMP or Sarin; hence, test calculations can be done more quickly. Furthermore, the mode of TCP adsorption (P=O−H−O bonding) is unambiguous.[38,39] Thus, it can be used to probe differences in the reactivity of various regions of the model cluster more easily than can a larger, polyfunctional molecule like DMMP.

The goal of the TCP studies is to assess the computational procedures before proceeding to the larger and more complex adsorbates. Experimental data, in the form of IR vibrational spectra, have been reported[38,39] for TCP adsorbed on high-surface-area (HSA) *a*-SiO₂ powders. The substrate preparation[40] used in these studies (vacuum annealing at 400−450 °C) yields a material with predominantly non-H-bonded Si−OH groups that may be either isolated or geminal. Structural data, obtained from microwave spectroscopy,[41] are also available for gas-phase TCP. These give r(P=O) = 1.455 ± 0.005 Å and r(P−Cl) = 1.989 ± 0.002 Å for the bond lengths and a ∠(Cl−P−Cl) bond

Figure 4. Schematic diagram showing the structure of Cl₃P=O adsorbed on the Si₅O₇H₈ cluster. The configuration shown results from geometry optimization at the B3LYP/6-31⁺G(2d,2p) level. The heavy green line shows the chemisorption bond.

angle of 103.7 ± 0.2°. In the present work, the corresponding values computed at the B3LYP/6-31⁺G(2d,2p) level are 1.460 and 2.036 Å and 103.6°.

4.1.1. Small-Cluster Model. As a further simplification, the present study began with the Si₅O₇H₈ cagelike cluster (Figure 4) described by Civalleri et al.[16] Among the different such clusters considered by this group this was the smallest that gave results for adsorption of NH₃, which were reasonably independent of cluster size. Table 1 shows that there is little difference among the ΔE_{ads}^{C} values for different basis sets. Both the TCP and the entire cluster were allowed to relax during optimization. From the computed vibrational modes (at the 6-31⁺G(d, p) level) of the adsorbate + cluster, bare cluster, and free adsorbate, $\Delta E_{ZPE} = +0.81$ kcal/mol was obtained after scaling the mode frequencies by a factor of 0.9632 (see above), resulting in $\Delta H_{ads}^{0} = -3.7$ kcal/mol. ΔE_{ZPE} is not expected to depend significantly on the basis set. Thus, the corresponding result for 6-31⁺G(2d,2p) was $\Delta E_{ZPE} = +0.70$ kcal/mol, giving $\Delta H_{ads}^{0} = -3.6$ kcal/mol. Hence, the ΔE_{ads}^{C} results remain nearly identical after further correction for ΔE_{ZPE}. Figure 4 shows the optimized structure for adsorbed TCP.

A calculation was also done at the 6-31⁺G(2d,2p) level for adsorption by P−Cl−H−O bonding. The result was $\Delta E_{ads} = -0.46$ kcal/mol and r(Cl−H) = 3.490 Å, indicating only a weak interaction. This is consistent with the smaller charge on Cl versus O, as shown by the atomic polarizability tensor[42] (APT) results for the free molecule in Table 2. ΔE_{ads} for this type of bonding corresponds to ~10% of the adsorption energy due to P=O−H−O interaction. The possibility of adsorption via an electrostatic interaction between the highly charged P atom (cf. Table 2) and the O of the Si−OH group was also investigated, but an even smaller interaction was found ($\Delta E_{ads} \approx -0.23$ kcal/mol, r(P−O) ≈ 4.389 Å). Furthermore, a structure of this type would be sterically hindered for the larger DMMP and Sarin molecules (cf. Figure 1).

Table 1 shows that proper treatment of anharmonicity (specifically, of the change in $\nu_e x_e$ caused by adsorption) is a significant factor in $\Delta\nu$(O−H), as noted in previous studies.[15,16,21,22] The results for the bare surface, ν_{01}(O−H) and $\nu_e x_e$, do not depend strongly on the choice of basis sets, but $\Delta\nu$(P=O) and $\Delta\nu_{01}$(O−H) are in somewhat better agreement with experiment for 6-31⁺G(2d,2p). The ν_{01}(O−H) and $\nu_e x_e$ results are close to those reported[16] by Civalleri et al. (3762 and 78 cm⁻¹, respectively) for the Si₅O₇H₈ cluster at the B3LYP/Dunning DZP(6d) level and with experimental results[38,39,43] for isolated OH groups on HSA *a*-SiO₂ powders. After adsorption of TCP, a $\nu_e x_e$ of about 106 cm⁻¹ is computed for the three basis sets.

In comparing observed and calculated results for $\Delta\nu_{01}$(O−H), it must be recalled that the former are obtained at room

TABLE 1: DFT/B3LYP Results for TCP Adsorption on the $Si_5O_7H_8$ Cluster for Different Basis Sets[a]

method	ΔE_{ads}[b]	r(P=O---H)	$\Delta\nu$(P=O)[c]	$\Delta\nu_{as}$(PCl$_3$)[c]	ν_{01}(O−H)[d]	$\nu_e x_e$[e]	$\Delta\nu_{01}$(O−H)[f]
6-31$^+$G(d, p)	−5.9 (−4.5)	1.867	−15	+13	3740 (3759)	76	−223 (−168)
6-311^{++}G(d, p)	−6.4 (−4.1)	1.880	−16	+8	3746 (3786)	74	−221 (−179)
6-31$^+$G(2d,2p)	−4.9 (−4.3)	1.897	−20	+13	3751 (3769)	77	−239 (−181)
Experiment[g]			−36	0	3747		−251
Experiment[h]			−33	+11	3747		−247
Experiment[i]					3745	85	

[a] ΔE_{ads} is in kcal/mol, r(P=O−H) is the H-bond distance in Å, and ν, $\nu_e x_e$, and $\Delta\nu$ are in cm^{-1}. [b] Values for ΔE_{ads}^C (the BSSE-corrected ΔE_{ads}) are in parentheses. [c] $\Delta\nu$(P=O) and $\Delta\nu_{as}$(PCl$_3$) are the frequency shifts (relative to the gas phase) obtained for purely harmonic potentials after scaling as described in the text. [d] ν_{01}(O−H) is the anharmonic SiO−H frequency for the bare cluster as described in the text. The value in parentheses is the frequency obtained for a purely harmonic potential after scaling. [e] Anharmonicity parameter for the bare cluster. After adsorption, $\nu_e x_e$ is about 106 cm^{-1} for the different basis sets. [f] $\Delta\nu_{01}$(O−H) is the change in ν_{01}(O−H) caused by adsorption of TCP. Numbers in parentheses are the corresponding results obtained after scaling for a purely harmonic potential. [g] Data for bare a-SiO$_2$ and for adsorbed TCP from ref 38 (recorded at room temperature). [h] Data for bare a-SiO$_2$ and for adsorbed TCP from ref 39 (recorded at RT). [i] Data for bare a-SiO$_2$ from ref 43 (recorded at RT). $\nu_e x_e = (2\nu_{01} - \nu_{02})/2$ was obtained from the reported ν_{01}(O−H) and ν_{02}(O−H) frequencies.

TABLE 2: APT Atomic Charges in Free Molecules[a]

molecule	P*=O	P=O*	R−O*	P−X*
Cl$_3$P=O	+2.10	−0.76		−0.45
DMMP	+2.12	−0.82	−1.00	
Sarin	+2.13	−0.84	−1.09	−0.67

[a] All values are obtained at the B3LYP/6-31$^+$G(2d,2p) level with an ultrafine integration grid. The asterisk marks the atom being described. R = CH$_3$− for DMMP and (CH$_3$)$_2$CH− for Sarin. X = Cl for TCP and F for Sarin.

temperature while the later pertain to $T = 0$. It has been shown experimentally[44] for NH$_3$ adsorbed on HSA a-SiO$_2$ powders that $\Delta\nu$(O−H) = −700 cm^{-1} at room temperature (RT) and −900 cm^{-1} at 4 °K. With large basis sets, a periodic−lattice model and the inclusion of anharmonicity, the DFT/B3LYP result[15] for $\Delta\nu_{01}$(O−H) is −733 cm^{-1}. After various corrections are applied, this becomes −633 cm^{-1}, which is still close to the experimental RT value but underestimates the $T = 0$ value. No IR data are available for TCP adsorbed on SiO$_2$ at cryogenic temperatures, but the results in ref 44 suggest that the apparent good agreement between theory and experiment for $\Delta\nu_{01}$(O−H) in Table 1 may be misleading. Nevertheless, the agreement is better when anharmonicity is explicitly included.

To determine whether explicit treatment of anharmonicity would also improve the agreement between the observed and calculated $\Delta\nu$(P=O), a similar analysis was done for this mode. Examination of the normal-mode displacements for TCP, either free or adsorbed on the Si$_5$O$_7$H$_8$ cluster, shows that the P=O stretch is essentially decoupled from other modes; hence, the approach outlined above is applicable. In this case, the anharmonicity is much smaller than for the O−H stretch. For free TCP, $\nu_e x_e = 7.0$ cm^{-1} for ν(P=O), using 6-31$^+$G(2d,2p) basis sets, vs 77 cm^{-1} (Table 1) for ν(O−H) of the bare Si−OH group. The approximation, noted above, of describing the ν(P=O) normal mode entirely in terms of displacement of the lighter atom is less valid here than in the case of ν(O−H). Nevertheless, the computed anharmonic ν_{01}(P=O) for free TCP, 1268 cm^{-1}, is closer to the experimental gas-phase value[38,39] of 1322 cm^{-1} than is the result (ν(P=O) = 1246 cm^{-1}) of scaling the purely harmonic frequency. However, the adsorption-induced shift obtained with explicit inclusion of anharmonicity, $\Delta\nu_{01}$(P=O) = −17 cm^{-1}, is negligibly different from the value of −20 cm^{-1} (Table 1) obtained simply by scaling the purely harmonic frequency shift. Thus the effect of adsorption on $\nu_e x_e$ appears to be much smaller for ν(P=O) than for ν(O−H).

Finally, Table 1 shows that all three models give reasonable results for $\Delta\nu_{as}$(PCl$_3$), the shift relative to the gas phase for the asymmetric PCl$_3$ stretching mode. This mode is doubly degenerate in the gas phase but splits by 3 to 6 cm^{-1} in the adsorbed

state (depending on the method of calculation) when the C_{3v} symmetry of the free molecule is eliminated. The shifts given in Table 1 are based on the average of the two frequencies for the adsorbed species.

4.1.2. Large-Cluster Model. The small cluster described above may appear adequate for describing the adsorption of TCP; however, deficiencies in this model will be identified below. In any case larger, polyfunctional molecules such as DMMP and Sarin require a model with multiple OH groups. Even for a relatively simple molecule like TCP, a realistic treatment of adsorption must allow the possibility of interaction with adjacent sites not directly bonded to the adsorbate.[35] Several tests of the adsorption of TCP on the large-cluster model will now be performed. These include a comparison of the high-OH-density (Figure 2a) and low-OH-density (Figure 3a,b) models, a comparison of isolated and geminal sites, and an assessment of the effects of the size of the ONIOM model system.

Table 3 shows results for TCP adsorption at the isolated Si−OH group of the model shown in Figure 2a. These were obtained after optimization using semiempirical low-level methods. Consistent results for ΔE_{ads} and r(P=O−H−O) were found only with a subsequent single-point calculation with RHF/3-21G for the low-level method. Without the single-point calculation, MNDO gives a shorter bond length but a smaller ΔE_{ads} than does PM3. In both cases, the optimized structure (not shown) gave no indication of interaction with sites other than the adsorption site. For example, the nearest adjacent OH site is located such that the resulting OH−O=P distance is 3.98 Å, and any other relevant distances (e.g., OH−Cl) are even greater.

In view of the results in Table 3, the q_{Si}^{model} values noted above and the discussions in refs 20 and 35, all subsequent ONIOM work will make use of RHF/3-21G as the low-level method. One adjustment was necessary, namely, the use of a 3-21G(d) basis set for the P atom. In the molecules of interest here, P is hypervalent, having one π- and three σ-bonds. This requires a higher degree of variational freedom (i.e., d-orbitals) in the P basis set, without which SCF convergence problems were often encountered. In the following (and in Table 3), 3-21G(d) for the P atom should be understood whenever reference is made to 3-21G basis sets for the low-level method.

Table 4 and Figure 5 show results for TCP adsorption at different sites, which indicate some significant points. First is the fact that for adsorption at the isolated Si−OH site of Figure 2a, ΔE_{ads} for optimization with RHF/3-21G as the low-level method (−9.5 kcal/mol) is close to the single-point result after optimization with MNDO as the low-level method (−10.1 kcal/mol, Table 3). This is consistent with previous results[35] for a different system (NH$_3$ adsorption on an alumi-

TABLE 3: Results for TCP Adsorption on Large-Cluster *a*-SiO$_2$ Models for Different ONIOM Methods[a]

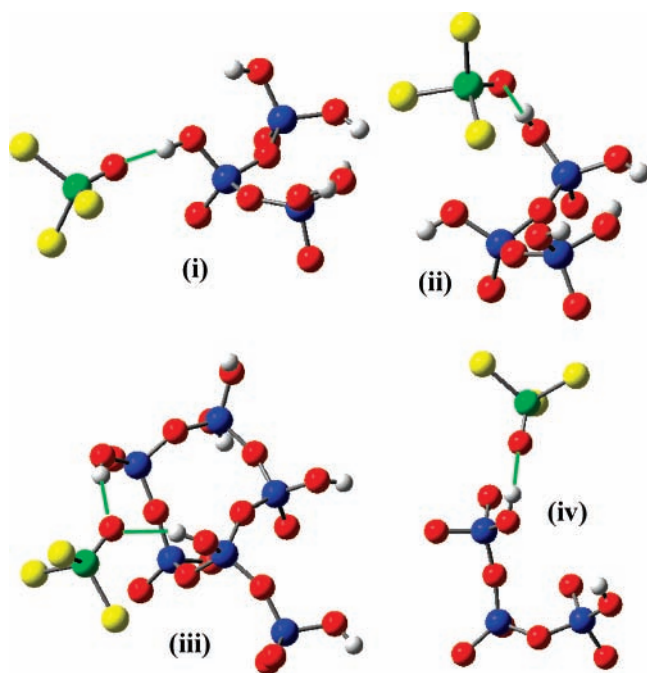| method	ΔE_{ads}[b]	$r(P{=}O\text{---}H{-}O)$
B3LYP/6-31$^+$G(2d,2p):PM3	−10.9 (−10.5)	2.001
B3LYP/6-31$^+$G(2d,2p):PM3//:RHF/3-21G[c]	−2.9 (−2.5)	
B3LYP/6-31$^+$G(2d,2p):MNDO	−5.8 (−5.3)	1.918
B3LYP/6-31$^+$G(2d,2p):MNDO//:RHF/3-21G	−10.1 (−9.7)	

[a] Energies are in kcal/mol; bond lengths are in Å. In all cases, adsorption occurs at the isolated OH of the model shown in Figure 2a. [b]Numbers in parentheses are the BSSE-corrected (ΔE_{ads}^{C}) values. The same ΔE_{BSSE} (+0.42 kcal/mol) is used in all cases because the high-level method is the same. [c]The notation means that the geometry was first optimized using B3LYP/6-31$^+$G(2d,2p) for the high-level and PM3 for the low-level method. Then a single-point calculation was done with RHF/3-21G as the low-level method (with 3-21G(d) for the P atom).

TABLE 4: Results for TCP Adsorption on Different *a*-SiO$_2$ Large-Cluster ONIOM Models[a]

model[b]	ΔE_{ads}[c]	$r(P{=}O\text{---}H{-}O)$
(i) isol OH (Figure 2a)	−9.5 (−9.0)	1.845
(ii) gem OH (Figure 2a)	−6.2 (−5.7)	1.877
(iii) isol OH; large model (Figure 3a)	−11.0 (−10.4)	2.148, 2.203[d]
(iv) isol OH; small model (Figure 3b)	−7.6 (−7.0)	1.804

[a] All calculations are done at the B3LYP/6-31$^+$G(2d,2p):RHF/3-21G level (with a 3-21G(d) basis set for the P atom). Energies are in kcal/mol, and bond lengths are in Å. [b]isol = isolated; gem = geminal. The structures are labeled (i), etc., to facilitate referencing in the text and in Figure 5. [c]Values in parentheses are ΔE_{ads}^{C} for ΔE_{BSSE} = +0.42 kcal/mol. [d]This structure exhibits H bonding between P=O and two Si−OH groups.

Figure 5. Optimized structure for TCP adsorbed at the Si−OH sites indicated in Table 4. The labels (i), etc., correspond to those in Table 4. For clarity, only the ONIOM model systems are shown, and each is in approximately the same orientation as in Figure 2a or 3a,b. The additional H atoms used as ONIOM "link" atoms are not shown. The heavy green lines show the dominant bonding interactions.

nosilicate material) and serves as a useful test of the present computational procedure.

In all cases shown in Table 4, ΔE_{ads}^{C} is larger than the value of −4.3 kcal/mol found for the small Si$_5$O$_7$H$_8$ cluster (Table 1). This may be because of the rigidity of the Si$_5$O$_7$H$_8$ structure, which consists of fused siloxane rings with only three or four Si atoms, as opposed to the "loose" and open structure of the large-cluster model. This permits only limited relaxation in response to adsorption, even though the entire Si$_5$O$_7$H$_8$ cluster is unconstrained during optimization. In this context, one notes that of structures (i), (ii), and (iv) the most stable is structure

(i) in which adsorption occurs at the center of the fully relaxed subcluster. When only one Si−OH group is involved in H-bonding, geminal- and isolated-OH sites have been found[45] to give similar ΔE_{ads} values. Hence, the difference in ΔE_{ads} between (i) and (ii) is not thought to be due to the presence of the second, noninteracting geminal OH group in (ii).

The optimized structures in Figure 5 exhibit differing degrees of interaction between TCP and multiple OH sites. This emphasizes a basic difficulty in treating a disordered system with a small finite-cluster model. For example, (iii) shows a "bidentate" structure with H bonding between TCP and two Si−OH sites. This can be achieved only for a local geometry in which two such sites are present with the correct separation and relative orientation. Note that adsorption at the geminal site (ii) does not lead to this energetically most favorable bidentate structure. Other structures suggest a possible contribution from O−H−Cl−P interaction (not shown) involving OH sites outside of the ONIOM model system, although this should be relatively weak, as noted above. One structure, (ii), shows no indication of such interactions. None of these can be taken to represent a unique and universal model for TCP adsorption on *a*-SiO$_2$.

Taken together, the results in Tables 1 and 4 suggest that there is a requirement for a sufficiently flexible structure, one with adequate freedom to relax in the vicinity of the adsorption site and with an ONIOM model system that includes all sites that might be involved in adsorbate bonding. When these conditions are reasonably well-satisfied, there is not a great difference in ΔE_{ads} between structures with quite different geometries (e.g., (i) and (iii) in Figure 5). A more precise treatment of TCP adsorption would focus on a range of different adsorption sites, all modeled in accord with the criteria stated above. This would presumably decrease the spread in ΔE_{ads} values shown in Table 4. However, the main interest here is in the adsorption of DMMP and Sarin. Further refinements in the treatment of TCP adsorption are therefore not justified but the results obtained above will be applied to modeling the adsorbates of interest.

Finally, the SiO−H stretching frequency was examined for the case of adsorption with the structure in Figure 5(i). For the bare cluster, $\nu_{01}(O{-}H)$ = 3744 and $\nu_e x_e$ = 77 cm^{-1} were obtained which are in good agreement with experiment (Table 1). Adsorption of TCP gave $\Delta\nu_{01}(O{-}H)$ = −267 cm^{-1}. A similar calculation for structure (ii), which has the smallest ΔE_{ads} of those shown in Figure 5, gave $\Delta\nu_{01}(O{-}H)$ = −260 cm^{-1}. These values (which pertain to $T = 0$) are slightly larger than the RT experimental result of about −250 cm^{-1} (Table 1). Bearing in mind the remarks made previously regarding the temperature dependence of $\Delta\nu_{01}(O{-}H)$, the agreement with experiment is reasonable.

It is useful to compare the results for ΔE_{ads}, $r(P{=}O{-}H{-}O)$, and $\Delta\nu_{01}(O{-}H)$ in Table 1 with those for structures (i), (ii), and (iv) given above and in Table 4. In all cases, $r(P{=}O{-}H{-}O)$ and $\Delta\nu_{01}(O{-}H)$, which directly reflect the strength of the H-bond interaction, are similar, whereas, the

ΔE_{ads} values differ. For molecules in solution, the Badger–Bauer relationship[12] predicts a strong and nearly linear increase in $\Delta\nu_{01}(O-H)$ with H-bond strength. The present results suggest that ΔE_{ads} depends on other factors in addition to the H-bond strength, such as relaxation at the adsorption site and possibly interaction of the adsorbate with adjacent sites. Thus, the small $Si_5O_7H_8$ cluster performs fairly well in describing the strength of a single H bond but not in predicting the adsorption energy.
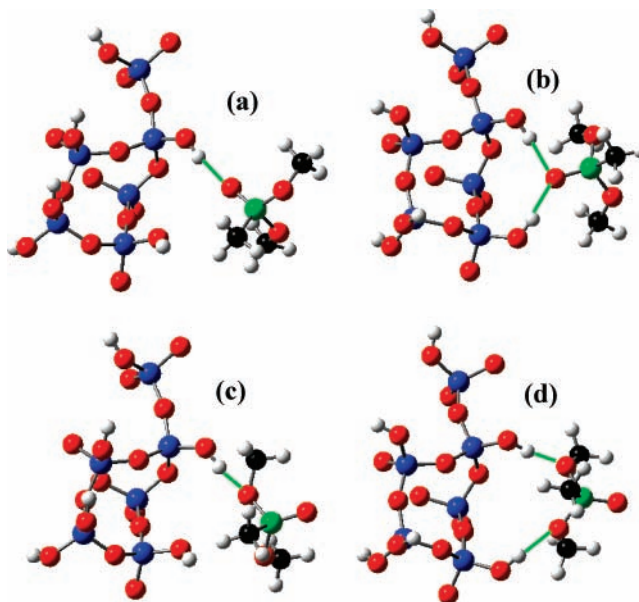
4.2. DMMP Adsorbed on a-SiO$_2$. The insights gained in the study of TCP adsorption will now be applied to the case of DMMP. The approach will be to use the large-cluster model to determine ΔE_{ads}, the adsorption geometry and $\Delta\nu_{01}(O-H)$ and to use the $Si_5O_7H_8$ cluster in computing the internal vibrational modes of adsorbed DMMP. The latter step is taken for two reasons. First, even with the use of analytical gradients, a complete normal-mode calculation for the large-cluster model is too computationally expensive. Second, the partial geometry optimization performed for the large-cluster model (see above) precludes an accurate calculation of the lower-energy modes of adsorbed DMMP because, unlike the SiO–H stretch, many of these are coupled to displacements of atoms in the cluster. The foregoing discussion of TCP indicates that reasonable results are to be expected for the internal modes of an adsorbate bonded to the $Si_5O_7H_8$ cluster. Experimental and theoretical results for the conformation and vibrational modes of gas-phase DMMP have been discussed in ref 10. As in ref 10, the gas-phase DMMP conformer (Figure 1b) used in the present work is the one identified previously[46] as the lowest in energy.

4.2.1. Experimental Results. The interaction of DMMP with a-SiO$_2$ HSA powder has been studied by Kanan and Tripp[38] using IR spectroscopy and by Henderson et al.[47] using temperature-programmed desorption and Auger electron spectroscopy. The IR results are interpreted in terms of non-dissociative adsorption via H-bond formation between isolated or geminal Si–OH sites and the two molecular CH$_3$O– groups. The P=O group is thought not to be directly involved in adsorption. The activation energy for desorption is estimated[47] to be ~16.9 kcal/mol.

The main effects in the IR spectrum that result from adsorption are the following:

(a) a shift of the SiO–H stretch by $\Delta\nu(O-H) = -524$ cm^{-1}, relative to the bare surface;

(b) a shift of the SiO–H bend by $\Delta\delta(O-H) \approx +160$ cm^{-1}, relative to the bare surface;

(c) a shift of the P=O stretch by $\Delta\nu(P=O) = -19$ cm^{-1}, relative to the gas-phase;

(d) little or no change in the $\nu_a(C-H)$ and $\nu_s(C-H)$ antisymmetric and symmetric stretches of the –OCH$_3$ groups;

(e) a weakening and/or broadening of the ν_s and ν_a symmetric and antisymmetric P–O–CH$_3$ stretching modes, relative to the gas phase, to the point of disappearance.

As a further point, it is noted that H bonding between DMMP and H$_2$O is found[48] both theoretically and experimentally to occur via a P=O–H–O linkage with experimental values of $\Delta\nu(P=O) = -17$ cm^{-1} and $\Delta\nu(O-H) = -203$ cm^{-1} for the symmetric stretching mode of H$_2$O. Studies[14,19] at the B3LYP/6-31$^+$G(d, p) level of the interaction between orthosilicic acid, Si(OH)$_4$, and the dimethyl phosphonate ion, [(CH$_3$O)$_2$PO$_2$]$^-$, also indicate an energetic preference for H bonding to the two lone O atoms versus to the methoxy O atoms. In IR spectroscopic studies of the interaction of DMMP with organic self-assembled monolayers terminated in OH tail groups[49] and with polymeric siloxane materials,[50] bonding is suggested to occur

Figure 6. Initial and final (optimized) structures for adsorbed DMMP. For clarity, only the molecule and the ONIOM model system (cf. Figure 3a) are shown. The additional H atoms used as ONIOM "link" atoms are not shown. Diagrams (a) and (c) show the initial structures, and (b) and (d) show the optimized structures. The heavy green lines show the dominant bonding interactions.

through P=O–H–O formation, which leads to shifts in $\nu(P=O)$ as large as -48 cm^{-1} relative to the gas phase.

Thus the interpretation proposed by Kanan and Tripp,[38] involving adsorption exclusively via the DMMP methoxy groups, differs from models put forth in connection with other similar systems. However, strong support for this interpretation comes from IR data[38] for the adsorption of (CH$_3$)$_x$Si(OCH$_3$)$_{4-x}$ ($x = 1$, 2, 3). The modes involving –OCH$_3$ groups behave identically to those in DMMP, although $\Delta\nu(O-H)$ is only -397 cm^{-1} versus -524 cm^{-1} for DMMP. In the case of DMMP, only one shifted SiO–H stretch is observed, not two as would be expected if adsorption involved both a strong bond to CH$_3$O– and a weak bond to P=O. It therefore appears that the surface chemistry of a-SiO$_2$ might differ from that of the model systems discussed above.

4.2.2. Computed Results. Calculations were done starting with a model in which adsorption occurs via a single P=O–H–O bond (Figure 6a) or a single (CH$_3$)(P)O–H–O bond (Figure 6c). As before, B3LYP/6-31$^+$G(2d,2p) was used for the ONIOM high-level method, and RHF/3-21G [3-21G(d) for P] was used for the low-level method. The a-SiO$_2$ model in all cases is that shown in Figure 3a. The results are summarized in Table 5. In the first case, rearrangement of the initial structure occurs to give a final optimized structure (Figure 6b) with bonding of the P=O to two Si–OH groups, as did TCP (Figure 5(iii)). The results obtained are $\Delta E_{ads} = -21.6$ kcal/mol ($\Delta E_{ads}^C = -20.0$ kcal/mol) and 1.916 and 1.936 Å for the two H-bond lengths. In the second case, the optimized structure (Figure 6d) shows a short H bond (1.783 Å) between one CH$_3$O– and an Si–OH group and a longer bond (2.134 Å) between the other CH$_3$O– and a second Si–OH. This is essentially the structure proposed by Kanan and Tripp.[38] The adsorption energy in this case is $\Delta E_{ads} = -15.1$ kcal/mol ($\Delta E_{ads}^C = -13.6$ kcal/mol). These ΔE_{ads}^C values are both larger than the corresponding result for TCP (-10.4 kcal/mol, Table 4) which is consistent with the experimental observation[38] that DMMP adsorbs more strongly on a-SiO$_2$ than does TCP. The ΔE_{ads}^C values are also close to the observed desorption

TABLE 5: Results for DMMP Adsorption on a-SiO$_2$[a]

	$\Delta E_{ads}^{C,b}$	$r(O\text{-}\text{-}\text{-}H)^{b,c}$	$\Delta\nu_{01}(O\text{-}H)^d$	$\Delta\delta(O\text{-}H)^e$	$\Delta\nu(P\text{=}O)^e$
Figure 6b	−20.0	1.916	−420	∼+257	−29
		1.936			
Figure 6d	−13.6	1.783	−423	∼+170	+7
		2.134			
experiment[f]			−524	∼+160	−19

[a] Energies are in kcal/mol, bond lengths are in Å, and frequencies are in cm⁻¹. [b]Values obtained for adsorption on the large-cluster model shown in Figure 3a. [c]Two H bonds are formed in either case (see text). The two H-bond lengths for each structure are tabulated. [d]Values obtained from an exact treatment of anharmonicity (see text) for adsorption on the large-cluster model shown in Figure 3a. Only the stronger (i.e., shorter) of the two H bonds is considered. [e]Values obtained for the small-cluster Si₅O₇H₈ model. The calculated harmonic values have been scaled by a factor of 0.9632 (see text). [f]Data from ref 38.

energy[47] of about 16.9 kcal/mol, and including a small ΔE_{ZPE} term (<1 kcal/mol, see above) would improve the agreement in the case of adsorption via the P=O group.

A calculation was also done starting with a structure (not shown) in which DMMP adsorbs via short H bonds (∼1.8 Å) between both CH₃O− groups and two isolated Si−OH groups. This was done in an effort to see if a more stable form of the structure shown in Figure 6d could be forced by starting closer to the desired final configuration. Early in the geometry optimization, the DMMP rearranged from the initial structure to one exhibiting an H bond to a single CH₃O− group and a second bond between another Si−OH and the P=O group. The resulting ΔE_{ads} was −10.1 kcal/mol, indicating a metastable (i.e., local minimum) configuration relative to those shown in Figure 6b,d. In effect, the H bond to either group (P=O or CH₃O−) interferes with optimum bonding to the other. It thus appears that the structure shown in Figure 6b is the most stable that can be achieved.

The relevant vibrational properties can now be studied (Table 5). Anharmonic $\Delta\nu_{01}(O\text{-}H)$ values for the structures shown in Figure 6b,d were obtained as described above. In either case, only the shorter (stronger) H bond was considered, and this gave $\Delta\nu_{01}(O\text{-}H) = -420$ cm⁻¹ (−423 cm⁻¹) for the structure in Figure 6b (Figure 6d). These are to be compared with the experimental value of $\Delta\nu_{01}(O\text{-}H) = -524$ cm⁻¹. As is typically found,[15,16,21] the calculated values (which are nearly identical for the two structures) underestimate somewhat the experimental result.

The internal vibrational modes of DMMP were computed for adsorption in either of the two possible configurations at the isolated Si−OH group of the Si₅O₇H₈ cluster (as discussed above). The calculation was done at the B3LYP/6-31⁺G(2d,2p) level with complete relaxation of both cluster and adsorbate. The ΔE_{ads} values were −9.7 and −4.8 kcal/mol, respectively, for H bonding to P=O and to CH₃O−. The H-bond lengths were 1.700 and 1.853 Å, respectively. As was found for TCP adsorption, the small-cluster energies are significantly smaller in magnitude than those for the larger and more flexible cluster with two H bonds per DMMP. Nevertheless, DMMP adsorbed via the P=O group is again found to be the more favorable of the two structures, which is consistent with the large-cluster results given above. $\Delta\nu(P\text{=}O)$ for H bonding to the P=O group is −29 cm⁻¹, whereas for H bonding to the CH₃O− group it is +7 cm⁻¹. The experimental result is $\Delta\nu(P\text{=}O) = -19$ cm⁻¹. Thus, H bonding to the CH₃O− group gives a $\Delta\nu(P\text{=}O)$ of the wrong sign.

For gas-phase DMMP, the out-of-phase and in-phase $\nu(C\text{-}O)$ modes are computed (at the B3LYP/6-31⁺G(2d,2p) level)

to lie at 1007 and 1031 cm⁻¹, respectively, after scaling as described above. The corresponding experimental values[49] are 1050 and 1075 cm⁻¹. The absolute values differ somewhat from experiment, due to systematic errors[24] in the frequency calculation, but the difference between the in-phase and out-of-phase modes is practically identical in theory (24 cm⁻¹) and experiment (25 cm⁻¹).

For DMMP adsorbed via the P=O group, these modes show little or no shift in frequency (∼3 cm⁻¹). For adsorption via the CH₃O− group, $\nu(C\text{-}O)$ is at 980 cm⁻¹ for the H-bonded CH₃O− and 1025 cm⁻¹ for the free CH₃O−. This shift of 45 cm⁻¹ is not by itself expected to make the H-bonded C−O stretch undetectable in the IR spectrum. For either type of adsorption, examination of the normal mode atomic displacements shows that the C−O stretching modes are coupled to Si−O−Si bond-stretching "lattice modes" of the cluster and/or to the Si−O−H bending mode, all of which occur in about the same energy region. The coupling can be described as "strong" in the sense that the C−O stretching normal modes also involve large Si−O stretching and/or Si−O−H bending motions. This may account for the broadening seen experimentally[38] for the C−O stretching modes when either DMMP or (CH₃)$_x$Si(OCH₃)$_{4-x}$ is adsorbed on a-SiO₂. Thus the broadening of the C−O stretching modes is not necessarily an indication of H bonding to the O atom of the CH₃O− groups in DMMP.
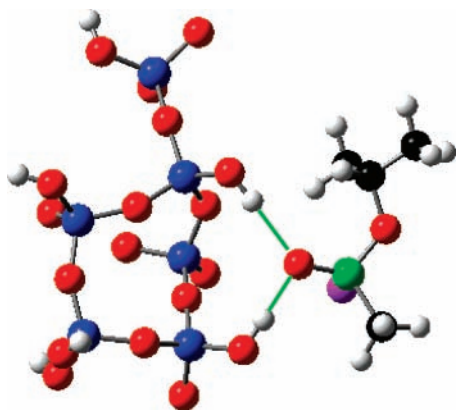
Table 5 also gives results for the effect of adsorption on $\delta(O\text{-}H)$, the frequency of the Si−O−H bending mode. An exact value for $\Delta\delta(O\text{-}H)$ is difficult to determine in the computational results because of strong coupling between this mode and the Si−O and C−O stretching modes, as discussed above. For the bare cluster, $\delta(O\text{-}H)$ is found at 832 cm⁻¹. For DMMP adsorbed via the P=O group, Si−O−H bending contributes significantly to several modes in the range of about 1002 to 1089 cm⁻¹. The highest of these appears to be almost pure Si−O−H bending. Using this value results in an estimate of $\Delta\delta(O\text{-}H) \approx +257$ cm⁻¹. In a sense, the mixing of Si−O−H bending with the C−O and Si−O stretching modes is the result of adsorption, which shifts the bending mode into the energy range of the stretches. Similar considerations for the case of adsorption via the CH₃O− group give $\Delta\delta(O\text{-}H) \approx +170$ cm⁻¹, based on the frequency of the mode that most closely approximates a pure Si−O−H bending motion. Although this result is very close to the experimental value (∼+160 cm⁻¹), the results for ΔE_{ads}^C and for $\Delta\nu(P\text{=}O)$ continue to argue in favor of H bonding to the P=O group.

4.3. Sarin Adsorbed on a-SiO₂. There are, to our knowledge, no experimental studies of Sarin adsorbed on a-SiO₂. Michalkova et al.[9] have reported theoretical results for the interaction of Sarin with Si(OH)₄. Bonding occurs via O−H···O=P interaction (with an H-bond distance of 1.756 Å) accompanied by an additional interaction between an H of the −CH₃ group and the O of a second Si−OH group (at a distance of 2.657 Å). H bonding to the O atom of the iPr−O−P group is not found to be important. At the B3LYP/6-31G(d) level, $\Delta E_{ads}^C = -7.6$ kcal/mol is obtained. Experimental and theoretical results for the conformation and vibrational modes of free Sarin have been discussed in ref 10. The conformer used for gas-phase Sarin, shown in Figure 1c, is identical to that used in ref 10. This is the second-lowest-energy conformer,[51,52] which lies <0.2 Kcal/mol above the absolute lowest-energy conformer. Different Sarin conformers are defined in terms of rotations about the iPr−O− and −O−P bonds, and different enantiomers of the same conformer, obtained by interchanging the F and phosphonyl O atoms, are isoenergetic.[51]

TABLE 6: Results for Sarin Adsorption on *a*-SiO₂[a]

H-bond site	ΔE_{ads}	ΔE_{ads}^{C}	r(H---X)[b]
P=**O**	−21.4	−19.9	1.779, 2.133
iPr−**O**−P−**F**	−11.3	−9.5	1.944 (O), 2.146 (F)
P−**F**	−12.4	−11.2	2.198, 2.413

[a] Energies are in kcal/mol, and bond lengths are in Å. The atom shown in bold is the one involved in H bonding. [b] X≡O or F. For P=**O** and P−**F**, H bonds are formed to two Si−OH groups. For iPr−**O**−P−**F**, one H bond forms to the O atom and another to the F atom.

Figure 7. Similar to Figure 6b but showing the optimized structure for Sarin adsorbed via H bonding to the P=O group. The violet sphere is the F atom.

In the present work, three modes of adsorption were considered. These are H bonding to the O atom of the P=O or iPr−O−P group, as for DMMP, and also to the F atom. In each case, the large-cluster model (Figure 3a) is used, and the starting structure involves only one H bond (as in Figure 6a,c). The results for the final optimized structures are summarized in Table 6. As in the case of TCP and DMMP, the most stable structure (Figure 7) involves H bonding between the P=O group and two Si−OH groups. Adsorption via the F atom also involves H bonding between the F and two Si−OH groups but is less stable than bonding to P=O. The optimized structures were examined for the possibility of H bonds to other functional groups; however, all such interatomic distances were 3.2 Å or greater. In comparison to the H-bond distances shown in Tables 1, 4, and 6, this is considered to be too large for a significant contribution to ΔE_{ads}. The initial structure with a single H bond to the O atom of the iPr−O−P group rearranged during optimization to one with this H bond intact and with a second H bond between F and another Si−OH. However, this is again less stable than two H bonds to the P=O group. The vibrational properties, computed for the most stable optimized structure using the procedure described above, were $\Delta\nu_{01}(O-H) = -510$ cm^{-1} (for the shorter of the two H bonds) and $\Delta\nu(P=O) = -25$ cm^{-1}. Given the results for DMMP (Table 5), the computed $\Delta\nu_{01}(O-H)$ for Sarin probably underestimates the experimental value, and the computed $\Delta\nu(P=O)$ probably overestimates the experimental value.

5. Summary

Ab initio QC calculations have been performed to study the interaction of TCP, DMMP, and Sarin via H bonding to Si−OH groups on the hydroxylated *a*-SiO₂ surface. The results are as follows.

(1) A small, cagelike cluster gives reasonable results for the vibrational spectrum of adsorbed TCP and DMMP. This includes the adsorption-induced red shift of the silanol ν(O−H) stretching mode when anharmonicity is treated explic-

itly. However, the adsorption energy is underestimated because of the rigidity of the model, which limits the extent of relaxation at the adsorption site, and to the omission of interactions between the adsorbate and more than one Si−OH.

(2) For the adsorbates studied here, an ONIOM treatment requires the use of an ab initio method (here RHF/3-21G) for the low level, rather than a semiempirical method. Including d orbitals in the low-level basis set (e.g., 3-21G(d)) is required for the adsorbate P atom.

(3) For all three species studied here, H-bond formation between the O atom of the P=O group and two Si−OH groups is the most energetically favorable adsorption mechanism. For DMMP and Sarin, H bonding to alkoxy O atoms is less favorable, as is H bonding to the Sarin F atom.

(4) The energetics and geometry of adsorption for DMMP and Sarin on *a*-SiO₂ depend on the local Si−OH environment. The bidentate P=O(−H−O)₂ structure is the dominant factor in adsorption. However, contributions from other, weaker interactions can be expected in real systems if the local Si−OH configuration is such that these effects are energetically feasible. H bonding to more than one functional group is seen in the present work for adsorption of DMMP in a metastable configuration with one H bond to the O atom of a CH₃−O−P group and a second to the P=O. It is also seen for Sarin adsorption (again in a metastable configuration) via the O atom of the iPr−O−P group, where a second H bond to the F atom also forms. Similar effects have also been observed in computational studies[3,4,9] of Sarin on other oxides.

(5) The characteristics of DMMP and Sarin with respect to adsorption on the *a*-SiO₂ surface are closely similar. In particular, the computed adsorption energies of the two species are virtually identical. Hence, DMMP is a good simulant for Sarin in this regard. It is not, however, to be concluded that the same is necessarily true for all adsorbent materials and under all conditions. For example, the effect of coadsorbed H₂O on the adsorption of DMMP or Sarin has not yet been analyzed, either computationally or experimentally. Furthermore, for adsorption on OH-free γ-Al₂O₃, which occurs via a different mechanism,[10] DMMP may interact somewhat more strongly than does Sarin.

References and Notes

(1) Wang, J.; Gu, J.; Leszczynski, J. *J. Phys. Chem. B* **2006**, *110*, 7567.
(2) Šečkute, J.; Menke, J. L.; Emnett, R. J.; Patterson, E. V.; Cramer, C. J. *J. Org. Chem.* **2005**, *70*, 8649.
(3) Michalkova, A.; Gorb, L.; Ilchenko, M.; Zhikol, O. A.; Shishkin, O. V.; Leszczynski, J. *J. Phys. Chem. B* **2004**, *108*, 1918.
(4) Michalkova, A.; Ilchenko, M.; Gorb, L.; Leszczynski, J. *J. Phys. Chem. B* **2004**, *108*, 5294.
(5) Hurley, M. M.; Wright, J. B.; Lushington, G. H.; White, W. E. *Theor. Chem. Acc.* **2003**, *109*, 160.
(6) Zheng, F.; Zhan, C.-G.; Ornstein, R. L. *J. Chem. Soc., Perkin Trans. 2* **2001**, 2355.
(7) Glukhovtsev, M. N.; Bach, R. D.; Nagel, C. J. *J. Phys. Chem. A* **1998**, *102*, 3438.
(8) Patterson, E. V.; Cramer, C. J. *J. Phys. Org. Chem.* **1998**, *11*, 232.
(9) Michalkova, A.; Martinez, J.; Zhikol, O. A.; Gorb, L.; Shishkin, O. V.; Leszczynska, D.; Leszczynski, J. *J. Phys. Chem. B* **2006**, *110*, 21175.
(10) Bermudez, V. M. *J. Phys. Chem. C* **2007**, *111*, 3719.

(11) Michalkova, A.; Paukku, Y.; Majumdar, D.; Leszczynski, J. *Chem. Phys. Lett.* **2007**, *438*, 72.

(12) Scheiner, S. *Hydrogen Bonding - A Theoretical Perspective*; Oxford: New York, 1997.

(13) Frisch, M. J.; Trucks, G. W.; Schlegel, H. B.; Scuseria, G. E.; Robb, M. A.; Cheeseman, J. R.; Montgomery, Jr., J. A.; Vreven, T.; Kudin, K. N.; Burant, J. C.; Millam, J. M.; Iyengar, S. S.; Tomasi, J.; Barone, V.; Mennucci, B.; Cossi, M.; Scalmani, G.; Rega, N.; Petersson, G. A.; Nakatsuji, H.; Hada, M.; Ehara, M.; Toyota, K.; Fukuda, R.; Hasegawa, J.; Ishida, M.; Nakajima, T.; Honda, Y.; Kitao, O.; Nakai, H.; Klene, M.; Li, X.; Knox, J. E.; Hratchian, H. P.; Cross, J. B.; Bakken, V.; Adamo, C.; Jaramillo, J.; Gomperts, R.; Stratmann, R. E.; Yazyev, O.; Austin, A. J.; Cammi, R.; Pomelli, C.; Ochterski, J. W.; Ayala, P. Y.; Morokuma, K.; Voth, G. A.; Salvador, P.; Dannenberg, J. J.; Zakrzewski, V. G.; Dapprich, S.; Daniels, A. D.; Strain, M. C.; Farkas, O.; Malick, D. K.; Rabuck, A. D.; Raghavachari, K.; Foresman, J. B.; Ortiz, J. V.; Cui, Q.; Baboul, A. G.; Clifford, S.; Cioslowski, J.; Stefanov, B. B.; Liu, G.; Liashenko, A.; Piskorz, P.; Komaromi, I.; Martin, R. L.; Fox, D. J.; Keith, T.; Al-Laham, M. A.; Peng, C. Y.; Nanayakkara, A.; Challacombe, M.; Gill, P. M. W.; Johnson, B.; Chen, W.; Wong, M. W.; Gonzalez, C.; Pople, J. A.; *Gaussian 03*, revision C.02; Gaussian, Inc., Wallingford CT, 2004.

(14) Murashov, V. V.; Leszczynski, J. *J. Mol. Struc.* **2000**, *529*, 1.

(15) Civalleri, B.; Ugliengo, P. *J. Phys. Chem. B* **2000**, *104*, 9491.

(16) Civalleri, B.; Garrone, E.; Ugliengo, P. *Langmuir* **1999**, *15*, 5829.

(17) Civalleri, B.; Garrone, E.; Ugliengo, P. *J. Phys. Chem. B* **1998**, *102*, 2373.

(18) Pelmenschikov, A. G.; Morosi, G.; Gamba, A. *J. Phys. Chem. A* **1997**, *101*, 1178.,

(19) Murashov, V. V.; Leszczynski, J. *J. Phys. Chem. A* **1999**, *103*, 1228.

(20) Roggero, I.; Civalleri, B.; Ugliengo, P. *Chem. Phys. Lett.* **2001**, *341*, 625.

(21) Civalleri, B.; Casassa, S.; Garrone, E.; Pisani, C.; Ugliengo, P. *J. Phys. Chem. B* **1999**, *103*, 2165.

(22) Senchenya, I. N.; Garrone, E.; Ugliengo, P. *J. Mol. Struct.* **1996**, *368*, 93.

(23) Van der Maelen Uría, J. F.; García-Granda, S.; Menéndez-Velázquez, A. *Am. J. Phys.* **1996**, *64*, 327.

(24) Irikura, K. K.; Johnson, R. D., III; Kacker, R. N. *J. Phys. Chem. A* **2005**, *109*, 8430.

(25) Andersson, M. P.; Uvdal, P. *J. Phys. Chem. A* **2005**, *109*, 2937.

(26) Van Ginhoven, R. M.; Jónsson, H.; Corrales, L. R. *Phys. Rev. B* **2005**, *71*, 024208.

(27) Van Ginhoven, R. M.; Jónsson, H.; Peterson, K. A.; Dupuis, M.; Corrales, L. R. *J. Chem. Phys.* **2003**, *118*, 6582.

(28) Ma, Y.; Foster, A. S.; Nieminen, R. M. *J. Chem. Phys.* **2005**, *122*, 144709.

(29) Takei, T.; Kato, K.; Meguro, A.; Chikazawa, M. *Colloid Surf., A* **1999**, *150*, 77.

(30) Stewart, J. J. P. *J. Comput.-Aided Mol. Des.* **1990**, *4*, 1.

(31) Hair, M. L. *Infrared Spectroscopy in Surface Chemistry*; M. Dekker: New York, 1967.

(32) Zhuravlev, L. T. *Langmuir* **1987**, *3*, 316.

(33) (a) Dapprich, S.; Komáromi, I.; Byun, K. S.; Morokuma, K.; Frisch, M. J. *J. Mol. Struct.* **1999**, *461−462*, 1. (b) Vreven, T.; Morokuma, K. *J. Comput. Chem.* **2000**, *21*, 1419.

(34) Dewar, M. J. S.; Thiel, W. *J. Am. Chem. Soc.* **1977**, *99*, 4899.

(35) Solans-Monfort, X.; Sodupe, M.; Branchadell, V.; Sauer, J.; Orlando, R.; Ugliengo, P. *J. Phys. Chem. B* **2005**, *109*, 3539.

(36) Bartlett, R. J.; McClellan, J.; Greer, J. C.; Monaghan, S. *J. Comput.-Aided Mater. Des.* **2006**, *13*, 89.

(37) Dovesi, R.; Roetti, C.; Freyria-Fava, C.; Aprà, E.; Saunders, V. R.; Harrison, N. M. *Philos. Trans. R. Soc. London, Ser. A* **1992**, *341*, 203.

(38) Kanan, S. M.; Tripp, C. P. *Langmuir* **2001**, *17*, 2213; **2002**, *18*, 722.

(39) Morrow, B. A.; Lang, S. J.; Gay, I. D. *Langmuir* **1994**, *10*, 756.

(40) Tripp, C. P.; Hair, M. L. *Langmuir* **1991**, *7*, 923.

(41) Li, Y. S.; Chen, M. M.; Durig, J. R. *J. Mol. Struct.* **1972**, *14*, 261.

(42) Cioslowski, J. *J. Am. Chem. Soc.* **1989**, *111*, 8333.

(43) Kustov, L. M.; Borovkov, V. Yu.; Kazansky, V. B. *J. Catal.* **1981**, *72*, 149.

(44) Tsyganenko, A. A.; Babaeva, M. A. *Opt. Spectrosk.* **1983**, *54*, 1117; *Opt. Spectrosc.* **1983**, *54*, 665 (English translation).

(45) Ferrari, A. M.; Ugliengo, P.; Garrone, E. *J. Phys. Chem.* **1993**, *97*, 2671.

(46) Suenram, R. D.; Lovas, F. J.; Plusquellic, D. F.; Lesarri, A.; Kawashima, Y.; Jensen, J. O.; Samuels, A. C. *J. Mol. Spectrosc.* **2002**, *211*, 110.

(47) Henderson, M. A.; Jin, T.; White, J. M. *J. Phys. Chem.* **1986**, *90*, 4607.

(48) Ault, B. S.; Balboa, A.; Tevault, D.; Hurley, M. *J. Phys. Chem. A* **2004**, *108*, 10094.

(49) (a) Bertilsson, L.; Potje-Kamloth, K.; Liess, H.-D.; Liedberg, B. *Langmuir* **1999**, *15*, 1128. (b) Bertilsson, L.; Potje-Kamloth, K.; Liess, H.-D.; Engquist, I.; Liedberg, B. *J. Phys. Chem. B* **1998**, *102*, 1260. (c) Bertilsson, L.; Engquist, I.; Liedberg, B. *J. Phys. Chem. B* **1997**, *101*, 6021.

(50) Ferguson-McPherson, M. K.; Low, E. R.; Esker, A. R.; Morris, J. R. *J. Phys. Chem. B* **2005**, *109*, 18914.

(51) Walker, A. R. H.; Suenram, R. D.; Samuels, A.; Jensen, J.; Ellzy, M. W.; Lochner, J. M.; Zeroka, D. *J. Mol. Spectrosc.* **2001**, *207*, 77.

(52) Kaczmarek, A.; Gorb, L.; Sadlej, A. J.; Leszczynski, J. *Struct. Chem.* **2004**, *15*, 517.